Article

Interaction of Cyanine-D112 with Binary Lipid Mixtures: Molecular Dynamics Simulation and Differential Scanning Calorimetry Study

Jinhui Li, Poornima Kalyanram, Seyedalireza Rozati, Viviana Monje-Galvan, and Anju Gupta*

Read Online

ACCESS | Metrics & More | Article Recommendations | SI Supporting Information

ABSTRACT: This comprehensive molecular dynamics (MD) simulation and experimental study investigates the lipid bilayer interactions of dye D112 for potential photodynamic therapy (PDT) applications. PDT involves formation of a reactive oxidant species in the presence of a light sensitive molecule and light, interrupting cellular functions. D112 was developed as a photographic emulsifier, and we hypothesized that its combined cationic and lipophilic nature can render a superior photosensitizing property—crucial in various light therapies. The focus of this study is to elucidate the binding and insertion mechanisms of D112 with mixed lipid bilayers of anionic dipalmitoyl-phosphatidylserine (DPPS) and zwitterionic dipalmitoyl-phosphatidylcholine (DPPC) lipids to resemble cancer cell membranes. Our studies confirm initial electrostatic binding between the positively charged moieties of D112 and negatively charged lipid headgroups. Additionally, MD simulations combined with differential scanning calorimetry (DSC) studies confirm that D112-lipid interactions are governed by enthalpy-driven nonclassical hydrophobic effects in the membrane interior. It was further noted that despite the electrostatic preference of D112 toward the anionic lipids, D112 molecules colocalized on DPPC-rich domains after insertion. Atomistic level MD studies point toward two possible insertion mechanisms for D112: harpoon and flip. Further insights from the simulation showcase the interactions of low and high aggregates of D112 with the bilayer as the concentration of D112 increases in solution. The size of aggregates modulates the orientation and degree of insertion, providing important information for future studies on membrane permeation mechanisms.
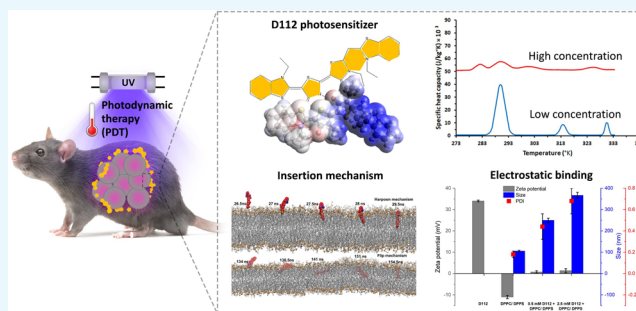
1. INTRODUCTION

Since the beginning of ancient civilizations, light has been used for the treatment of various diseases.[1] In the modern age, the efficacy of light treatment is enhanced using chemical agents, particularly in the treatment of skin cancer, vitiligo, psoriasis, acne vulgaris, and rosacea.[2−11] One such treatment is photodynamic therapy (PDT) which is currently being used as an alternative treatment for the control of malignant diseases. PDT involves a photosensitizer molecule which, upon being excited by light of respective wavelength, reacts with oxygen in the cells to generate reactive oxidant species (ROS) in target tissues causing cell death.[12−14] Therefore, the overall efficacy of PDT is dependent on the photochemical and cellular uptake properties of the photosensitizer molecule.[15−17]

The degree of the membrane disruption by the photosensitizer is of particular importance to optimize the cytotoxicity in the PDT process and has triggered the search for new photosensitizers.[15−21] Hydrophobic photosensitizer molecules are known to insert and diffuse across the membranes; while they bind efficiently onto the surface of the membrane, their uptake occurs via assisted delivery or endocytosis.[22,23] Porphyrins represent first-generation water-soluble photosensitizer molecules discovered in the 1970s that were further mixed with dimers and oligomers to improve their selectivity

and photosensitizing potential. However, their applications were limited by their lower chemical purity and poor cell penetration.[24,25] This led to the discovery of the second generation of photosensitizers in the 1980s that involved porphyrin derivatives including benzoporphyrin, texaphyrins, and synthetic photosensitizers such as bacteriochlorin analogues and phthalocyanine, thiopurine derivatives, and chlorin.[26−29] The current third generation of photosensitizers is being developed to improve their bioavailability and selectivity through conjugation with biomolecules such as nucleic acids and proteins and their precise delivery through nanomaterials.[30−33] Most photosensitizer molecules are hydrophobic in nature with the tendency to aggregate in an aqueous environment that limits their PDT efficiency.[34−36]

We previously investigated the development and investigation of third-generation PSs by two strategies, one by designing a
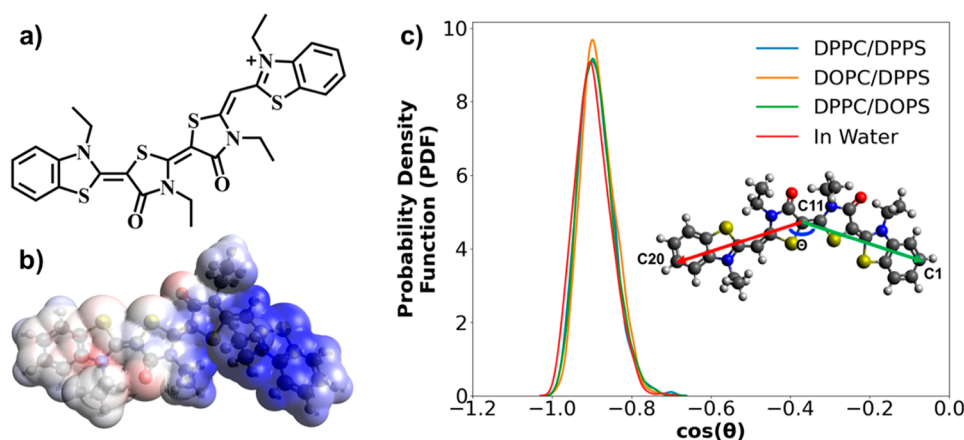
Figure 1. a) Molecular structure of cyanine dye-D112, b) D112 surface charge map, and c) D112 intramolecular kink angle distribution in water and in membrane bilayers.

lipid-based nanocarrier and another through modification of the first- and second-generation photosensitizer molecules.[37−41] We studied the dipalmitoylphosphatidylcholine (DPPC)/cholesterol (90/10) liposomal encapsulation of riboflavin that yielded a cell inhibition of 78% cell inhibition in the presence of blue light at a low encapsulation efficiency of 24%.[37] Another study involved encapsulation of the choline-based hydrophobic 2-[1-hexyloxyethyl]-2-devinyl pyropheophorbide-alpha (HPPH) photosensitizer in liposomes comprised of photopolymerizable diacetylene phosphatidylcholine lipids/polyethylene glycol (PEG) liposomes. Different molecular weights of PEG were tested at various concentrations with the lipids. *In vivo* studies demonstrated high serum stability and superior PDT efficacy with animal survival with no tumor recurrence up to 100 days.[38] We also investigated newly synthesized amphiphilic coumarin comprising of aminomethylcoumarin (AMC) conjugated with alkyl chains comprising of 5, 9, and 12 carbon atoms from AMC-C_n. Our results showed the highest uptake with AMC-C_{12} due to electrostatic binding between AMC and lipid headgroups followed by insertion of C_{12} chains in the lipid bilayer.[40]

Herein, we present the mechanism of interaction of cyanine-D112 with a DPPC/DPPS (85/15 by mol %) lipid mixture for the potential applications in PDT. D112 belongs to a class of delocalized hydrophobic cations and was developed for its use in photographic emulsions; it has further been shown to have anticancer cell activity *in vitro*.[42] Since the key property of the neoplastic cells is the changes in their lipid metabolism leading to abnormal cell membrane composition, this work primarily focuses on the interaction of D112 with the phospholipid membrane. DPPC and DPPS were chosen based on several reports[43−46] that suggest that the phosphatidylcholine lipids govern the proliferation rate and phosphatidylserine undergoes prominent changes to an extent that they could potentially be considered as cancer biomarkers.[47−49] Since phosphatidylserine lipids are anionic in nature, it is hypothesized that D112 will strongly bind to these lipid headgroups, and its lipophilicity will drive its insertion and lateral diffusion in the lipid bilayer. We performed zetapotential measurements to confirm the strong electrostatic binding between the D112 molecules and negatively charged phosphatidylserine headgroups. Additionally, since phosphatidylcholine is a zwitterionic lipid, it is postulated that the negatively charged moieties also participate in the electrostatic binding with cationic D112.

The initial electrostatic binding of the D112 molecules on the lipid bilayer surface followed by the formation of lipid-D112 aggregates was confirmed by changes in hydrodynamic size, zeta potential, and polydispersity index. Furthermore, the insertion and aggregation of D112 molecules in the lipid bilayer were investigated and validated using molecular dynamics (MD) simulation and differential scanning calorimetry (DSC) studies. MD simulations identified two insertion modes, *harpoon* and *flip*, depending on the portion of the D112 molecule to first interact with the DPPC/DPPS lipid bilayer. Additionally, the following features are noted on the interaction between D112 and mixed bilayer lipids from simulation: a) D112 resides vertically inside the leaflet, with its lipophilic region always pointing toward the bilayer center and the positively charged region next to the lipid headgroups in the binding leaflet, and b) D112 molecules prefer to localize to regions rich in neutral lipid headgroups once inside the membrane, like phosphatidylcholine (PC). This observation is in alignment with the phase separation observed in DSC studies that was employed to determine the bilayer order and packing, fluidity, phase transition behavior, and the location of D112 in the bilayer. Additionally, preliminary insights on the role of unsaturated lipids on their interactions with D112 were investigated using bilayers comprised of unsaturated dioleoyl lipids DOPC and DOPS. These later simulations demonstrate the presence of double bonds in the lipid tails, or unsaturation degree of the membrane core, has a limited effect on the binding and insertion mechanisms of D112.

There is an evident need to shorten the time to repurpose and reposition drugs with known pharmacokinetics and antimicrobial properties to mitigate current and future global disease outbreaks. This work represents a novel and alternative pathway to exploit pigments and dyes used for photographic emulsions as potential photosensitizers for various light therapies. The combined experimental and simulation approaches presented in this work can be leveraged to characterize mechanisms of binding, insertion, and translocation of photosensitive molecules. Such an integrated approach can be employed toward a cost-effective and systematic discovery of photosensitizers for photodynamic cancer therapy.

2. RESULTS AND DISCUSSION

2.1. Molecular Structure Analysis of D112. The chemical structure of D112 is shown in Figure 1a along with its corresponding charge map in Figure 1b; positively and
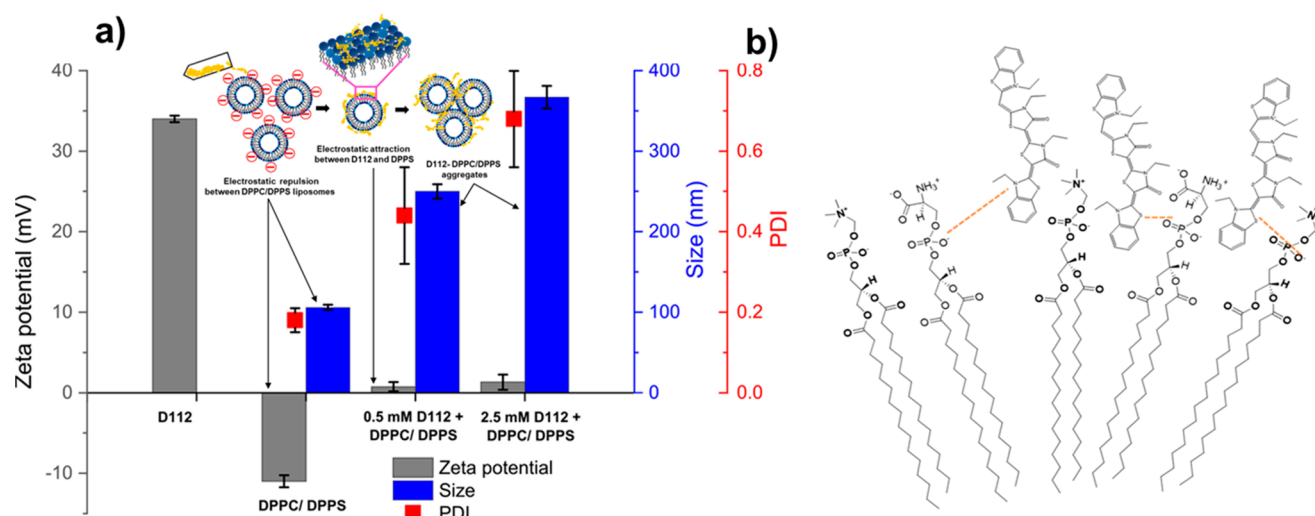
Figure 2. a) Comparison of changes in the zeta potential, hydrodynamic diameter, and polydispersity index (PDI) of DPPC/DPPS liposomes upon electrostatic binding with D112 at 317.15 K. Also shown schematically are the aggregation of DPPC/DPPS-D112 and b) schematic representation of D112 electrostatic interactions with the two lipid species.

negatively charged regions are represented in blue and red, respectively. D112 is a polar molecule due to its delocalized lipophilic cations and the cyanine backbone; it was hypothesized that the asymmetry plays a key role in its interaction with mixed lipid bilayers. Figure 1c shows the distribution of the intramolecular kink angle, defined as shown in the inset of the plot. The sharp peak represents the rigidity of D112, which remains unchanged whether the molecule is in water or interacting with lipid bilayers around 155° (or a cosine of −0.49). The root mean square deviation (RMSD) and root mean square fluctuation (RMSF) analyses in Figure S1 show fluctuations of the heavy atoms in D112. The molecule is not flexible and retains its spatial configuration even during insertion; as expected, the methyl carbons fluctuate more.

2.2. Electrostatic Binding and Insertion Mechanisms.
A Zetasizer Nano was used to examine the changes in the size and zeta potential of the 10 mM DPPC/DPPS liposomes upon addition of D112 molecules at 0.5 mM and 2.5 mM concentrations at gel phase (298.15 K) and fluid phase (317.15 K) temperatures[50] as summarized in Figure 2a. The zeta potential of just DPPC liposomes was measured to be 0.78 ± 0.50 mV,[51] which increased to 1.02 ± 0.23 mV in the presence of D112. The zeta potential of DPPC/DPPS liposomes in the absence of D112 was recorded as −11 mV[40] and as 35 mV for the D112 molecules suspended in lactic acid. Upon addition of D112 at 0.5 mM and 2.5 mM concentrations, the zeta potential of DPPC/DPPS liposomes increased to 0.739 ± 0.57 mV and 1.32 ± 0.95 mV, respectively. This transition in the zeta potential is a consequence of electrostatic binding between the negatively charged serine headgroup of DPPS[40,51] and the cyanine group in D112 molecules as depicted in Figure 2b along with a probable minor contribution from electrostatic binding with the negative phosphate moieties of DPPC.

The physical stability of liposomes is dependent on their lipid composition.[52−54] DPPC zwitterionic liposomes tend to aggregate; however, the presence of charged lipids such as DPPS impedes the aggregation through electrostatic repulsion. The measured hydrodynamic diameters of DPPC liposomes were approximately 150 nm and 125 nm for DPPC/DPPS liposomes with a low PDI of 0.21 obtained over 4 weeks. Electrostatic binding of D112 molecules on the liposome surface

resulted in the formation of D112-liposome aggregates shown schematically in Figure 2a. This aggregation is also represented by the large hydrodynamic diameters obtained for DPPC/DPPS liposomes in the presence of 0.5 mM and 2.5 mM concentrations of D112 measured in the fluid phase. D112 binding to liposomes is predominantly driven by the enthalpy change, and this nonclassical hydrophobic effect is the consequence of the differences between the bulk water and the hydrophobic lipid bilayer core.

The electrostatic binding was also confirmed in simulation trajectories. D112 molecules initially bind to the lipid bilayer via electrostatic interactions between the positively charged region of D112 and the negatively charged headgroups of DPPS. This is observed in all the replicas performed in this study for both systems with a single D112 or multiple molecules. Upon binding the membrane surface, D112-lipid interactions are modulated by hydrophobic interactions, which result in the insertion of D112 into the bilayer core. From our simulations, we characterized two insertion modes: harpoon and flip insertion. Table S1 lists the insertion mode and duration for all the replicas with a single D112 molecule; the harpoon insertion mode is significantly shorter than the flip insertion mode. Despite their different mechanisms, both result in the same and final orientation of D112 molecules in the hydrophobic core of the bilayer as discussed below. Figure 3a contains snapshots of sample systems showing the sequence of motions during each insertion mode, and Figure S2 shows the time series of insertion and final tilt angles of D112 for all the replicas with a single molecule. Movies 1 and 2 in the Supporting Information showcase these mechanisms for a single D112 molecule from its first contact with the bilayer and subsequent insertion.

The harpoon insertion mechanism, shown in Figure 3a, is a rapid process that involves vertical insertion of D112 in the lipid bilayer with its neutral tail pointing downward and into the binding leaflet. The positively charged end remains near the membrane surface, as it prefers to interact with the phosphate region of lipids as well as polar water molecules near the membrane interface. On the other hand, the flip insertion, shown in Figure 3b, is more complex and takes between four and five times longer to complete than the harpoon mechanism. Electrostatic interactions still drive the initial contact between
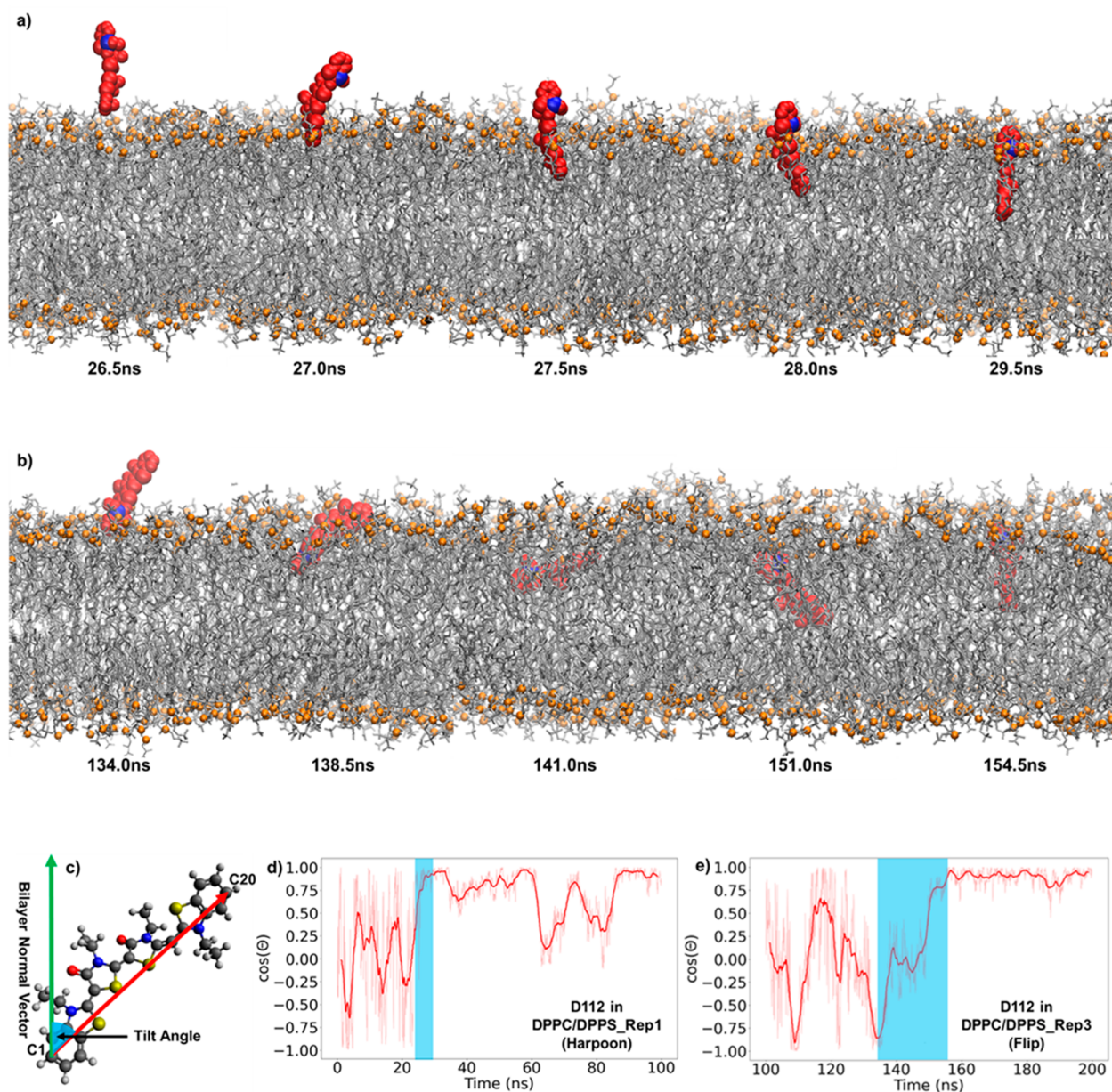
Figure 3. D112 insertion mechanisms observed in MD simulations. (a) Harpoon mechanism, showing rapid anchoring in the vertical orientation, and (b) flip mechanism, following a slower U-shape trajectory. Blue spheres in the red D112 molecules represent positively charged nitrogen atoms, and orange spheres represent phosphorus atoms in the membrane lipids. (c) Schematic of the tilt angle of the ring plane of D112 with respect to the lipid bilayer normal vector, the z-axis in these simulations. Time series of the tilt angle for the (d) harpoon and (e) flip insertion. The light blue region indicates the duration of the insertion process.

D112 and the lipid headgroups, yet the positively charged end of the D112 molecules enters first into the hydrophobic core and returns to the bilayer surface following a U-shaped trajectory inside the binding leaflet, effectively flipping its orientation from the center of the bilayer back to the surface. Table S1 summarizes the insertion mode and duration time frame for each replica of the systems with a single D112 molecule. The harpoon and flip insertion mechanisms were further differentiated by examining the tilt angle of D112 molecules during and at the end of the process, as shown in Figure 3c. The harpoon insertion lasts between 3 and 5 ns, while the flip insertion occurs past the initial 100 ns and takes nearly 20 ns to complete, as shown in highlighted regions in Figures 3d and 3e, respectively.

2.3. Insights on Low and High Order D112 Aggregates in Mixed Bilayers. Based on MD simulation studies involving multiple D112 molecules, monomers and their aggregates insert into the bilayer differently. Formation of low and high order D112 aggregates was observed in the water as well as inside the lipid bilayer. Table S2 summarizes the D112 aggregates formed in the different replicas. For instance, within the first 10−20 ns of the simulations, D112 formed dimers in the water phase. In accordance with the relative distance between the positively charged N atoms in each monomer, the dimers were classified as parallel or antiparallel as shown in Figure 4a. In antiparallel dimers, the positively charged end, shown in blue, is on opposite ends of the dimer; while in a parallel dimer, the positively charge ends are on the same side of the dimer. This is also evident from
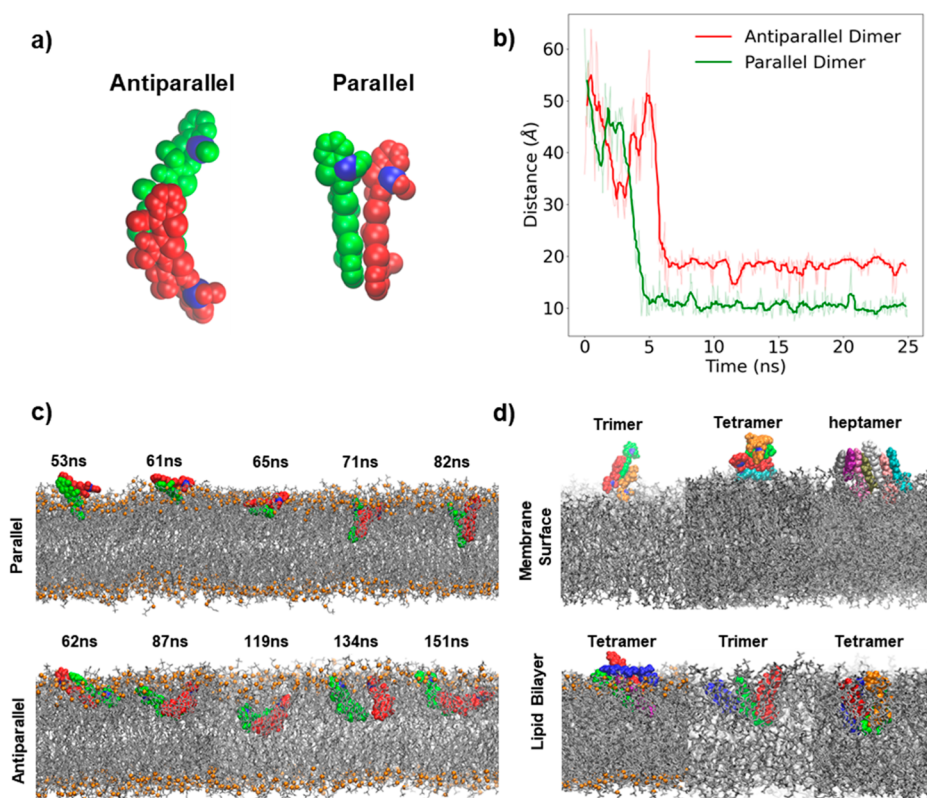
Figure 4. D112 aggregates. Dimers (a) in the antiparallel and parallel conformations. Blue spheres indicate the positively charged atom in the molecule. (b) Time series of the distance between the positively charged N atoms in D112 showing dimer formation. (c) Insertion of a parallel dimer (top) and an antiparallel dimer (bottom) into a bilayer. (d) High order D112 aggregates and their location with respect to the bilayer.

the larger N−N distance between D112 monomers in the antiparallel dimers, as seen in Figure 4b. Movies 3 and 4 in the Supporting Information illustrate D112 dimer formations in these two conformations. Parallel and antiparallel dimers interact with lipids through significantly different mechanisms. The insertion of parallel dimers occurs within the first 30−40 ns of the trajectory, with the center of mass of the molecule 10 Å below the phosphate region of the membrane lipids at the end of the simulation, whereas antiparallel dimers do not fully embed into the lipid bilayer but interact with the lipid phosphate groups horizontally at the membrane interface.

In the simulations with 15 D112 molecules, monomers and parallel and antiparallel dimers were found inside the bilayer (refer to Figure S3). Parallel dimers enter bilayers only via flip insertion as described in Figure 3b. None of the parallel dimers exhibited the harpoon insertion mechanism across the multiple simulation replicas, potentially due to its larger surface area and the absence of large-enough lipid packing defects on the membrane surface. Upon insertion, parallel dimers remained in the vertical position and well embedded in the hydrophobic core of the bilayer. In contrast, antiparallel dimers remained right below the phosphate layer of the membrane lipids in a nearly horizontal orientation as shown in Figure 4c. This was also confirmed by the tilt angle distribution of the main axis of D112 dimers with respect to the bilayer normal. Parallel dimers displayed a narrow peak for a very small angle with respect to the bilayer, that is, a vertical orientation inside the membrane core. Conversely, the antiparallel dimers revealed a broad distribution corresponding to a rather flat orientation, parallel to the membrane surface (refer to Figure S4).

Our simulation studies provide insights on aggregate conformations; their location and orientation in the bilayer when D112 is present in higher concentrations are in agreement with the trends with DSC experiments. Among the higher order D112 aggregates, only trimers and tetramers penetrated past the phosphate headgroup region of the lipids into the hydrophobic core of the bilayer as depicted in Figure 4d. Heptamers cannot insert into the bilayer due to their large size and hydrophilic character and spatial arrangement. This behavior has also been reported for other small amphiphilic molecules and their interactions with bilayers, such as statins.

2.4. Preferred Localization of D112 in Mixed Lipid Bilayers. DSC was used to study the changes in melting behavior, phase transitions, and domain formations in DPPC/DPPS (85/15 mol %) mixed bilayers in the presence of D112 at varying concentrations. The melting temperatures of pure DPPC and DPPS are reported to be 315.15 and 328.15 K, respectively. Additionally, the effects of annealing on the bilayer phase behavior in the presence of D112 were investigated by subjecting the samples to five subsequent heating and cooling cycles. Annealing was performed to study the thermal stresses induced in the bilayer and the effects on the insertion degree of D112. The phase transition temperatures examined in this study were used as references to determine the temperatures for the simulation. The simulated systems were also checked to ensure the bilayer remained in the fluid phase throughout the simulation, especially for the DPPC/DPPS system. All the simulations were carried out at temperatures above the transition temperature observed from DSC studies.

Upon addition of 0.5 mM D112, the heat capacity associated with the melting peak of the DPPC/DPPS mixture increased,
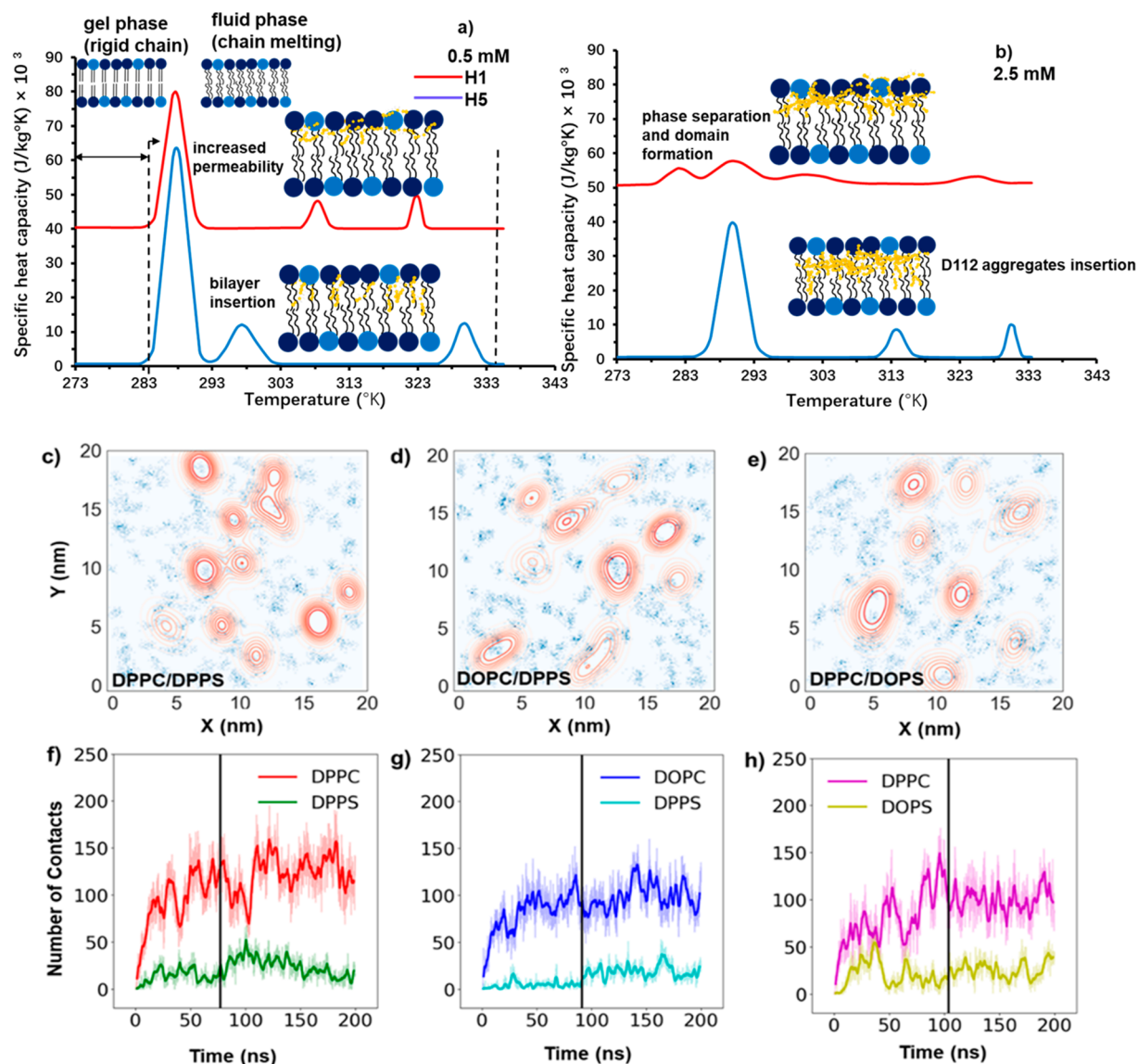
Figure 5. (a,b) DSC plots of DPPC/DPPS liposomes in the presence of D112 molecules at different concentrations. Heating cycles 1 and 5 are colored in red and blue, respectively. The second rows show the density maps for phosphatidylserine lipids (15% mol) in the lipid mixture models, a representation of the lateral distribution of lipids in each membrane during the last 50 ns of simulation of the systems with 15 D112 molecules for the (c) DPPC/DPPS, (d) DOPC/DPPS, and (e) DPPC/DOPS models. Each density map has the corresponding time series of D112-lipid contacts below (f−h); a contact was determined by counting the number of lipids of a given species within 0.5 nm of D112 molecules. The black line in the contact plots indicates the time where all D112 molecules were inserted in the bilayer core.

and the peak sharpened during the first heating cycle as shown in Figure 5a. The smaller peaks seen around 319.15 K and 330.15 K correspond to the melting peaks of pure DPPC and DPPS, respectively. These smaller peaks indicate a phase separation between the lipids due to the presence of D112 molecules in the outer leaflet, shown schematically. Five subsequent heating cycles exhibited no significant changes in the transition temperature other than broadening of the melting peaks with a minor shoulder on the right, suggesting deeper insertion of D112 into the lipid alkyl tails causing further phase separation. In contrast, addition of 2.5 mM D112 led to a shift of the melting peak from 315.25 K to 316.75 K, as seen in Figure 5b. This peak was also accompanied by smaller peaks at higher temperatures, representing the melting peaks of pure DPPC and DPPS lipids because of phase separation. A distinct pattern was observed during the fifth heating cycle in this case, suggesting phase domain formations in the bilayer due to deeper penetration of

D112 by virtue of its hydrophobicity. This is attributed to a large number of D112 molecules accumulating in the lipid bilayer core due to subsequent heating cycles that influenced the fluidity of the bilayer.

While a single D112 preferred to colocalize in the PC-rich region in the bilayer upon insertion, simulations with multiple D112 molecules demonstrated aggregation patterns corresponding to the experimental observations. Figure 5c−e shows the lipid density maps of the membrane models: DPPC/DPPS, DOPC/DPPS, and DPPC/DOPS, respectively. The dark blue regions indicate the average position of PS lipids during the last 50 ns of the respective trajectory, while the red contour maps show the relative location of the 15 D112 molecules inserted into different membrane models. Under each lateral density map are the corresponding time series for contacts between D112 and each lipid species. D112 lipid contacts were determined by counting the number of lipids of a given species within 5 Å from

Table 1. Summary of Various Systems Used in MD Simulation Studies

lipid mixture system	no. of atoms	no. of D112	no. of lipid molecules	no. of water molecules	temp (K)	counter ions # K+
DPPC/DPPS (85/15 mol %)	172678	1	300	31717	335	89
	173675	5	300	31960	335	85
	313236	15	600	52437	335	165
DOPC/DPPS (85/15 mol %)	165775	1	300	28056	310	89
	165683	5	300	27936	310	85
	370113	15	600	68676	310	165
DPPC/DOPS (85/15 mol %)	159526	1	300	27093	315	89
	159461	5	300	26982	315	85
	352572	15	600	65069	315	165

the heavy atoms of D112. Most D112 molecules ultimately localize into the PC-rich regions after their preliminary insertion into the bilayer; insertion usually takes places near the interface between the PC-rich and PS-rich regions. These observations are consistent with the two melting peaks corresponding to pure DPPC and DPPS shown in Figures 5a and 5b.

It is important to note this study considered symmetric membrane bilayers containing only two lipid species. Though this is an oversimplification of the complex lipid landscape in cell membranes, it is the first step to systematically characterize the role of the lipid chemical structure on the interactions of small molecules with the bilayer. Due to the nature of the simulations that were set up to run with periodic boundary conditions, this study did not examine the effect of accumulation of D112 molecules in a single leaflet, which would correspond to the outer leaflet of the liposomes considered in the experimental setting; this process warrants future studies. In this work, we provide a pathway to explore existing dyes and pigments for their therapeutic applications. The current study provides a comprehensive investigation of the binding and interaction mechanisms of D112 molecules with model lipid membranes via experiment and simulation.

3. CONCLUSION

This preliminary work investigated the interaction of the hydrophobic D112 photoemulsifier with lipid bilayers by applying computational and experimental approaches. Contrary to hydrophilic photosensitizers that are dependent on assisted delivery or endocytosis for their internalization, it has been demonstrated that the degree of insertion of hydrophobic photosensitizer molecules is of great significance to optimize their performance in light therapies. In the context of PDT, it is postulated that at the onset of administration, D112 aggregates can form ROS with the phospholipids in the plasma membrane even before they enter the cytosol, which may reduce the overall duration of the PDT. Our zeta potential measurements confirmed the expected electrostatic interaction between the negatively charged phosphatidylserine headgroups and D112 molecules. Similarly, MD simulations further provided insights on D112 aggregation and insertion into mixed lipid bilayers including saturated and unsaturated PC and PS lipids.

All-atom MD simulations found two interaction mechanisms with the bilayer core, namely *harpoon* or *flip* insertion. However, irrespective of the insertion method, the positively charged end of D112 molecules was found to be localized near the bilayer interface, while the lipophilic region remained embedded in the hydrophobic core of the membrane. DSC further confirmed the insertion of D112 at varying concentrations in DPPC/DPPS lipid bilayers through the formation of multiple phase-separated peaks during various heating cycles. Multiple D112 molecules

were further examined via simulations to mimic higher concentrations used in the DSC experiments. Throughout the multiple simulation replicas, low and high order D112 aggregates form and bind to the bilayer primarily through electrostatics. However, the degree and mode of insertion into the bilayer varies depending on the size of the aggregate.

The combined experimental and simulation approaches presented in this work can be adopted as a rapid-vetting strategy in the repurposing of dyes and pigments as photosensitizers for various light therapies. Future studies are required to fully investigate the binding behavior and aggregation patterns of D112 with complex lipid bilayers. Additionally, the accumulation of D112 in the outer leaflet and its effect on lateral sorting of lipids and domain formation remain to be studied. Elucidation of membrane permeation mechanisms in the context of PDT and drug delivery as well as *in vivo* and *in vitro* studies will certainly provide much needed knowledge to fully realize the applications of D112 in light therapy.

4. EXPERIMENTAL AND COMPUTATIONAL METHODS

4.1. Molecular Dynamics Simulations. Table 1 summarizes the lipid mixtures of DPPC/DPPS, DOPC/DPPS, and DPPC/DOPS that were built for the all-atom MD studies using CHARMM-GUI Membrane builder and Solution builder.[55−59] The additional lipid mixtures used in our simulation studies were selected to examine the effect of lipid tail unsaturation and headgroup charge on binding and insertion of D112. Coordinates for a single D112 molecule were built using ChemDraw 19.0 8[60] and then solvated in CHARMM-GUI, which provides parameters from CHARMM General Force Field (CGenFF) for the molecule.[61−63] This system was equilibrated for 50 ns in water to allow the D112 molecule to stabilize. The membrane models were relaxed following the CHARMM-GUI 6-step protocol and further equilibrated for 50 ns before positioning D112 molecules in the solvent. The number of D112 molecules in the aqueous phase was varied to examine dynamics with increasing concentration. One, five, and 15 D112 molecules were positioned between 10 and 20 Å away from the membrane interface and performed in triplicate for 200 ns (refer to Figure S5). The ratios between zwitterionic and anionic lipids were maintained at 85/15 mol %, varying the percentage of double bonds in the lipid tails in the different models. For the simulations with one and five D112 molecules, the membrane bilayers contain 300 lipids per leaflet; whereas for the systems with 15 D112 molecules, the bilayers are comprised of 600 lipids per leaflet to allow sufficient surface area for D112 molecules to diffuse freely and allow bulk membrane regions.

All systems were rendered neutral using K+ ions, and simulations were run using the GROMACS simulation package, CHARMM36m force field parameters,[63−65] and periodic

boundary conditions. NPT dynamics was run with a time step of 2 fs, temperature was kept constant with the Berendsen thermostat at 310 K or 335 K to ensure the bilayer remained in the fluid phase, and pressure was set at 1 bar and barostat, respectively.[66] Nonbonded interactions were modeled using a Lennard-Jones potential with a force-switching function between 10 and 12 Å, and long-range electrostatics were evaluated using Particle Mesh Ewald.[67] The LINCS algorithm was used to constrain bonds with hydrogen atoms in GROMACS.[68] Snapshots included in this work were generated using the Visual Molecular Dynamics (VMD) package,[69] and internal GROMACS modules, MDAnalysis,[70] and MDTraj[71] were used for analysis. All trajectories were computed with resources available at the Center for Computational Research (CCR) at the University at Buffalo.[72]

4.2. Reagents and Liposome Preparation. Cyanine-D112 was a gift sample from Dr. Kenneth Reed, Visiting Research Scientist, Rochester Institute of Technology. Lactic acid (≥98% purity) was purchased from Sigma-Aldrich. DPPC and DPPS lipids at >99% purity were supplied by Avanti Polar Lipids (Alabaster, AL). DPPC/DPPS liposomes of ratio 85/15 mol % were prepared at 1 mM concentration using the thin film hydration method followed by extrusion through polycarbonate membranes of pore sizes approximately 100 nm as described previously.[51] The cyanine-D112 solution was made in lactic acid at concentrations of 0.5 mM and 2.5 mM. The D112 solution was added to the preformed DPPC/DPPS liposomes.

4.3. Light Scattering Measurements. Dynamic light scattering (DLS) and zeta potential experiments were recorded using a Malvern Nano-ZS instrument. The measurements were made at a 173° backscatter angle in a SARSTEDT polystyrene cuvette in triplicate. The zeta potential measurements were done using a DTS1070 folded capillary cell. The zeta potential of the liposomes was measured before and after adding D112. The size and zeta potential measurements were performed at gel phase (298.15 K) and fluid phase (317.15 K) temperatures.

4.4. Differential Scanning Calorimetry. Nano differential scanning calorimetry (DSC) experiments were performed by adding D112 to 1 mM DPPC/DPPS liposomes at 0.5 mM and 2.5 mM concentrations in a 300 μL cell volume. The samples were annealed with five alternating heating and cooling cycles in the range of 298.15–343.15 K at a rate of 1 K/min.

■ ASSOCIATED CONTENT

ⓢ Supporting Information

The Supporting Information is available free of charge at https://pubs.acs.org/doi/10.1021/acsomega.1c07378.

> Harpoon insertion mechanism into model bilayer (Movie S1) (MP4)
>
> Flip insertion mechanism into model bilayer (Movie S2) (MP4)
>
> Dimerization of D112 molecules in parallel conformation (Movie S3) (MP4)
>
> Dimerization of D112 molecules in antiparallel conformation (Movie S4) (MP4)
>
> RMSD and RMSF of heavy atoms in D112 molecules in water and membrane bilayers (Figure S1); distance time series between COM of D112 and phosphate group of lipids and final tilt angle of molecule inside bilayer upon insertion (Figure S2); inserted D112 monomers and dimers in DPPC/DPPS membrane model (Figure S3); tilt angle distribution of inserted D112 dimers (Figure

S4); initial configuration of D112-mixed lipid bilayer (Figure S5); insertion occurrences across replicas for systems with single D112 as estimated from D112-phospholipid headgroup distance time series (Table S1); and number of D112 aggregates per replica at different points in trajectory (Table S2) (PDF)

■ AUTHOR INFORMATION

Corresponding Author

Anju Gupta — *Department of Mechanical, Industrial and Manufacturing Engineering, University of Toledo, Toledo, Ohio 43606, United States;* ⓘ orcid.org/0000-0001-5378-9496; Phone: +1(413)-530-8213; Email: anju.gupta@utoledo.edu

Authors

Jinhui Li — *Department of Chemical and Biological Engineering, University at Buffalo, Buffalo, New York 14260, United States*

Poornima Kalyanram — *Department of Mechanical, Industrial and Manufacturing Engineering, University of Toledo, Toledo, Ohio 43606, United States*

Seyedalireza Rozati — *Department of Mechanical, Industrial and Manufacturing Engineering, University of Toledo, Toledo, Ohio 43606, United States*

Viviana Monje-Galvan — *Department of Chemical and Biological Engineering, University at Buffalo, Buffalo, New York 14260, United States;* ⓘ orcid.org/0000-0002-9202-782X

Complete contact information is available at:
https://pubs.acs.org/10.1021/acsomega.1c07378

Author Contributions

J.L.: investigation, visualization, data curation, formal analysis, writing, review, and editing. P.K.: investigation. S.R.: investigation and data curation. V.M.G.: supervision, methodology, review, and editing. A.G.: conceptualization, investigation, supervision, writing, review, and editing.

Notes

The authors declare no competing financial interest.

■ ACKNOWLEDGMENTS

■ ABBREVIATIONS

DLS	dynamic light scattering
DSC	differential scanning calorimetry
DOPC	1,2-dioleoyl-*sn*-glycero-3-phosphocholine
DOPS	1,2-dioleoyl-*sn*-glycero-3-phospho-L-serine
DPPC	dipalmitoylphosphatidylcholine
DPPS	dipalmitoylphosphatidylserine
MD	molecular dynamics
PC	phosphatidylcholine
PS	phosphatidylserine
PDF	probability density function
PDI	polydispersity index
PDF	probability density function
PDT	photodynamic therapy
ROS	reactive oxidant species

VMD   Visual Molecular Dynamics

■ REFERENCES

(1) Daniell, M. D.; Hill, J. S. A History of Photodynamic Therapy. *Aust. N. Z. J. Surg.* **1991**, *61* (5), 340−348.

(2) Giorgio, C. M.; Caccavale, S.; Fulgione, E.; Moscarella, E.; Babino, G.; Argenziano, G. Efficacy of Microneedling and Photodynamic Therapy in Vitiligo. *Dermatol. Surg.* **2019**, *45* (11), 1424−1426.

(3) Tandon, Y. K.; Yang, M. F.; Baron, E. D. Role of Photodynamic Therapy in Psoriasis: A Brief Review. *Photodermatol. Photoimmunol. Photomed.* **2008**, *24* (5), 222−230.

(4) Zhao, B.; He, Y.-Y. Recent Advances in the Prevention and Treatment of Skin Cancer Using Photodynamic Therapy. *Expert Rev. Anticancer Ther.* **2010**, *10* (11), 1797−1809.

(5) Rahimi, H.; Zeinali, R.; Tehranchinia, Z. Photodynamic Therapy of Vitiligo: A Pilot Study. *Photodiagnosis Photodyn. Ther.* **2021**, *36*, 102439.

(6) Agostinis, P.; Berg, K.; Cengel, K. A.; Foster, T. H.; Girotti, A. W.; Gollnick, S. O.; Hahn, S. M.; Hamblin, M. R.; Juzeniene, A.; Kessel, D.; Korbelik, M.; Moan, J.; Mroz, P.; Nowis, D.; Piette, J.; Wilson, B. C.; Golab, J. Photodynamic Therapy of Cancer: An Update. *CA. Cancer J. Clin.* **2011**, *61* (4), 250−281.

(7) Fritsch, C.; Goerz, G.; Ruzicka, T. Photodynamic Therapy in Dermatology. *Arch. Dermatol.* **1998**, *134* (2), 207−214.

(8) Kalka, K.; Merk, H.; Mukhtar, H. Photodynamic Therapy in Dermatology. *J. Am. Acad. Dermatol.* **2000**, *42* (3), 389−413.

(9) Choi, Y. M.; Adelzadeh, L.; Wu, J. J. Photodynamic Therapy for Psoriasis. *J. Dermatol. Treat.* **2015**, *26* (3), 202−207.

(10) Babilas, P.; Landthaler, M.; Szeimies, R.-M. Photodynamic Therapy in Dermatology. *Eur. J. Dermatol.* **2006**, *16* (4), 340−348.

(11) Ruiz-Rodriguez, R.; Sanz-Sánchez, T.; Córdoba, S. Photodynamic Photorejuvenation. *Dermatol. Surg.* **2002**, *28* (8), 742−744.

(12) Macdonald, I. J.; Dougherty, T. J. Basic Principles of Photodynamic Therapy. *J. Porphyr. Phthalocyanines* **2001**, *05* (02), 105−129.

(13) Wang, J.; Yi, J. Cancer Cell Killing via ROS: To Increase or Decrease, That Is the Question. *Cancer Biol. Ther.* **2008**, *7* (12), 1875−1884.

(14) Dąbrowski, J. M. Chapter Nine - Reactive Oxygen Species in Photodynamic Therapy: Mechanisms of Their Generation and Potentiation. In *Advances in Inorganic Chemistry*; van Eldik, R., Hubbard, C. D., Eds.; Inorganic Reaction Mechanisms; Academic Press: 2017; Vol. 70, pp 343−394, DOI: 10.1016/bs.adioch.2017.03.002.

(15) Castano, A. P.; Demidova, T. N.; Hamblin, M. R. Mechanisms in Photodynamic Therapy: Part One—Photosensitizers, Photochemistry and Cellular Localization. *Photodiagnosis Photodyn. Ther.* **2004**, *1* (4), 279−293.

(16) Berlanda, J.; Kiesslich, T.; Engelhardt, V.; Krammer, B.; Plaetzer, K. Comparative in Vitro Study on the Characteristics of Different Photosensitizers Employed in PDT. *J. Photochem. Photobiol., B* **2010**, *100* (3), 173−180.

(17) Dąbrowski, J. M.; Pucelik, B.; Regiel-Futyra, A.; Brindell, M.; Mazuryk, O.; Kyzioł, A.; Stochel, G.; Macyk, W.; Arnaut, L. G. Engineering of Relevant Photodynamic Processes through Structural Modifications of Metallotetrapyrrolic Photosensitizers. *Coord. Chem. Rev.* **2016**, *325*, 67−101.

(18) Castano, A. P.; Demidova, T. N.; Hamblin, M. R. Mechanisms in Photodynamic Therapy: Part Two—Cellular Signaling, Cell Metabolism and Modes of Cell Death. *Photodiagnosis Photodyn. Ther.* **2005**, *2* (1), 1−23.

(19) Chen, W.-H.; Luo, G.-F.; Zhang, X.-Z. Recent Advances in Subcellular Targeted Cancer Therapy Based on Functional Materials. *Adv. Mater.* **2019**, *31* (3), 1802725.

(20) Weyergang, A.; Selbo, P. K.; Berstad, M. E. B.; Bostad, M.; Berg, K. Photochemical Internalization of Tumor-Targeted Protein Toxins. *Lasers Surg. Med.* **2011**, *43* (7), 721−733.

(21) Sharman, W. M.; van Lier, J. E.; Allen, C. M. Targeted Photodynamic Therapy via Receptor Mediated Delivery Systems. *Adv. Drug Delivery Rev.* **2004**, *56* (1), 53−76.

(22) Abedin, F.; Ye, Q.; Spencer, P. Hydrophilic Dyes as Photosensitizers for Photopolymerization of Dental Adhesives. *J. Dent.* **2020**, *99*, 103405.

(23) Wiehe, A.; Simonenko, E. J.; Senge, M. O.; RÖder, B. Hydrophilicity vs Hydrophobicity—Varying the Amphiphilic Structure of Porphyrins Related to the Photosensitizer m-THPC. *J. Porphyr. Phthalocyanines* **2001**, *5* (10), 758−761.

(24) Bock, G. R.; Harnett, S. *Photosensitizing Compounds: Their Chemistry, Biology and Clinical Use*; John Wiley & Sons: 2008.

(25) Zhang, Q.; He, J.; Yu, W.; Li, Y.; Liu, Z.; Zhou, B.; Liu, Y. A Promising Anticancer Drug: A Photosensitizer Based on the Porphyrin Skeleton. *RSC Med. Chem.* **2020**, *11* (4), 427−437.

(26) Gomer, C. J. Preclinical Examination of First and Second Generation Photosensitizers Used in Photodynamic Therapy. *Photochem. Photobiol.* **1991**, *54* (6), 1093−1107.

(27) Yu, Y.; Anthony, S. M.; Zhang, L.; Bae, S. C.; Granick, S. Cationic Nanoparticles Stabilize Zwitterionic Liposomes Better than Anionic Ones. *J. Phys. Chem. C* **2007**, *111* (23), 8233−8236.

(28) Rovers, J. P.; et al. Effective treatment of liver metastases with photodynamic therapy, using the second-generation photosensitizer meta-tetra(hydroxyphenyl)chlorin (mTHPC), in a rat model. *Br. J. Cancer* **2021**, *81*, 600.

(29) Sternberg, E. D.; Dolphin, D. Second Generation Photodynamic Agents: A Review. *J. Clin. Laser Med. Surg.* **1993**, *11* (5), 233−241.

(30) Josefsen, L. B.; Boyle, R. W. Photodynamic Therapy: Novel Third-Generation Photosensitizers One Step Closer? *Br. J. Pharmacol.* **2008**, *154* (1), 1−3.

(31) Setaro, F.; Wennink, J. W. H.; Mäkinen, P. I.; Holappa, L.; Trohopoulos, P. N.; Ylä-Herttuala, S.; Nostrum, C. F. van; Escosura, A. de la; Torres, T. Amphiphilic Phthalocyanines in Polymeric Micelles: A Supramolecular Approach toward Efficient Third-Generation Photosensitizers. *J. Mater. Chem. B* **2020**, *8* (2), 282−289.

(32) Mfouo-Tynga, I. S.; Dias, L. D.; Inada, N. M.; Kurachi, C. Features of Third Generation Photosensitizers Used in Anticancer Photodynamic Therapy: Review. *Photodiagnosis Photodyn. Ther.* **2021**, *34*, 102091.

(33) Gualdesi, M. S.; Vara, J.; Aiassa, V.; Alvarez Igarzabal, C. I.; Ortiz, C. S. New Poly(Acrylamide) Nanoparticles in the Development of Third Generation Photosensitizers. *Dyes Pigments* **2021**, *184*, 108856.

(34) Wang, C.; Zhao, P.; Jiang, D.; Yang, G.; Xue, Y.; Tang, Z.; Zhang, M.; Wang, H.; Jiang, X.; Wu, Y.; Liu, Y.; Zhang, W.; Bu, W. In Situ Catalytic Reaction for Solving the Aggregation of Hydrophobic Photosensitizers in Tumor. *ACS Appl. Mater. Interfaces* **2020**, *12* (5), 5624−5632.

(35) Ricchelli, F. Photophysical Properties of Porphyrins in Biological Membranes. *J. Photochem. Photobiol., B* **1995**, *29* (2), 109−118.

(36) Konan, Y. N.; Gurny, R.; Allémann, E. State of the Art in the Delivery of Photosensitizers for Photodynamic Therapy. *J. Photochem. Photobiol., B* **2002**, *66* (2), 89−106.

(37) Gupta, A.; Kalyanram, P.; Stadler, I. Interaction of Riboflavin-5-Phosphate With Liposome Bilayers. *J. Nanotoxicology Nanomedicine JNN* **2018**, *3* (1), 49−59.

(38) Kalyanram, P.; Puri, A.; Gupta, A. Thermotropic Effects of PEGylated Lipids on the Stability of HPPH-Encapsulated Lipid Nanoparticles (LNP). *J. Therm. Anal. Calorim.* **2021**, DOI: 10.1007/s10973-021-10929-6.

(39) Kalyanram, P.; Puri, A.; Gupta, A. Understanding the Stealth Properties of PEGylated lipids: A Mini-Review. *International Journal of Lipids* **2021**, *1*, 1.

(40) Kalyanram, P.; Ma, H.; Nangia, S.; Marshall, S.; Cartaya, A.; Zimmerman, T.; Goudreau, C.; Stadler, I.; Gupta, A. Interaction of amphiphilic coumarin with DPPC/DPPS lipid bilayer: effects of concentration and alkyl tail length. *Phys. Chem. Chem. Phys.* **2020**, *22*, 15197.

(41) Kalyanram, P.; Hussein, N.; Tiwari, A.; Gupta, A. Insights on the Thermal and Physical Stability of the Modified Polymerizable

Liposomes for Improved Photoactivity. *International Journal of Lipids* **2020**, *1*, 21.

(42) Yang, N.; Weinfeld, M.; Lemieux, H.; Montpetit, B.; Goping, I. S. Photo-Activation of the Delocalized Lipophilic Cation D112 Potentiates Cancer Selective ROS Production and Apoptosis. *Cell Death Dis* **2017**, *8* (2), No. e2587.

(43) Ricchelli, F.; Jori, G.; Gobbo, S.; Tronchin, M. Liposomes as Models to Study the Distribution of Porphyrins in Cell Membranes. *Biochim. Biophys. Acta* **1991**, *1065* (1), 42−48.

(44) Gravier, J.; Korchowiec, B.; Schneider, R.; Rogalska, E. Interaction of Amphiphilic Chlorin-Based Photosensitizers with 1,2-Dipalmitoyl-Sn-Glycero-3-Phosphocholine Monolayers. *Chem. Phys. Lipids* **2009**, *158* (2), 102−109.

(45) de Morais, F. A. P.; Gonçalves, R. S.; Vilsinski, B. H.; de Oliveira, É. L.; Rocha, N. L.; Hioka, N.; Caetano, W. Hypericin Photodynamic Activity in DPPC Liposome. PART I: Biomimetism of Loading, Location, Interactions and Thermodynamic Properties. *J. Photochem. Photobiol., B* **2019**, *190*, 118−127.

(46) Pamin, K.; Połtowicz, J.; Kiełkowicz, J.; Hendrich, A. Interaction of Metalloporphyrins with Lipid Bilayers, a Calorimetric Study. *Curr. Top. Biophys.* **2011**, *34*, 11.

(47) Fernandis, A. Z.; Wenk, M. R. Lipid-Based Biomarkers for Cancer. *J. Chromatogr. B* **2009**, *877* (26), 2830−2835.

(48) Szlasa, W.; Zendran, I.; Zalesińska, A.; Tarek, M.; Kulbacka, J. Lipid Composition of the Cancer Cell Membrane. *J. Bioenerg. Biomembr.* **2020**, *52* (5), 321−342.

(49) Bandu, R.; Mok, H. J.; Kim, K. P. Phospholipids as Cancer Biomarkers: Mass Spectrometry-Based Analysis. *Mass Spectrom. Rev.* **2018**, *37* (2), 107−138.

(50) Gupta, A.; Mandal, D.; Ahmadibeni, Y.; Parang, K.; Bothun, G. Hydrophobicity Drives the Cellular Uptake of Short Cationic Peptide Ligands. *Eur. Biophys. J. EBJ.* **2011**, *40* (6), 727−736.

(51) Gupta, A. *Investigation of Interaction of Cationic Amphiphiles with Model Membranes and Their Application in Drug Delivery*. Diss. Masters Theses Campus Access, 2011, pp 1−198.

(52) Zheng, T.; Chen, Y.; Shi, Y.; Feng, H. High Efficiency Liposome Fusion Induced by Reducing Undesired Membrane Peptides Interaction. *Open Chem.* **2019**, *17* (1), 31−42.

(53) Nakhaei, P.; Margiana, R.; Bokov, D. O.; Abdelbasset, W. K.; Jadidi Kouhbanani, M. A.; Varma, R. S.; Marofi, F.; Jarahian, M.; Beheshtkhoo, N. Liposomes: Structure, Biomedical Applications, and Stability Parameters With Emphasis on Cholesterol. *Front. Bioeng. Biotechnol.* **2021**, *9*, 705886.

(54) Anderson, M.; Omri, A. The Effect of Different Lipid Components on the In Vitro Stability and Release Kinetics of Liposome Formulations. *Drug Deliv* **2004**, *11* (1), 33−39.

(55) Jo, S.; Kim, T.; Iyer, V. G.; Im, W. CHARMM-GUI: A Web-Based Graphical User Interface for CHARMM. *J. Comput. Chem.* **2008**, *29* (11), 1859−1865.

(56) Wu, E. L.; Cheng, X.; Jo, S.; Rui, H.; Song, K. C.; Dávila-Contreras, E. M.; Qi, Y.; Lee, J.; Monje-Galvan, V.; Venable, R. M.; Klauda, J. B.; Im, W. CHARMM-GUI Membrane Builder toward Realistic Biological Membrane Simulations. *J. Comput. Chem.* **2014**, *35* (27), 1997−2004.

(57) Jo, S.; Lim, J. B.; Klauda, J. B.; Im, W. CHARMM-GUI Membrane Builder for Mixed Bilayers and Its Application to Yeast Membranes. *Biophys. J.* **2009**, *97* (1), 50−58.

(58) Lee, J.; Patel, D. S.; Widmalm, G.; Im, W. CHARMM-GUI Membrane Builder for Complex Biological Membrane Simulations with Glycolipids and Lipoglycans. *J. Chem. Theory Comput.* **2019**, *15* (1), 775.

(59) Jo, S.; Kim, T.; Im, W. Automated Builder and Database of Protein/Membrane Complexes for Molecular Dynamics Simulations. *PLoS One* **2007**, *2* (9), No. e880.

(60) Cousins, K. R. Computer Review of ChemDraw Ultra 12.0. *J. Am. Chem. Soc.* **2011**, *133* (21), 8388.

(61) Lee, J.; Cheng, X.; Swails, J. M.; Yeom, M. S.; Eastman, P. K.; Lemkul, J. A.; Wei, S.; Buckner, J.; Jeong, J. C.; Qi, Y.; Jo, S.; Pande, V. S.; Case, D. A.; Brooks, C. L.; MacKerell, A. D.; Klauda, J. B.; Im, W.

CHARMM-GUI Input Generator for NAMD, GROMACS, AMBER, OpenMM, and CHARMM/OpenMM Simulations Using the CHARMM36 Additive Force Field. *J. Chem. Theory Comput.* **2016**, *12* (1), 405−413.

(62) Vanommeslaeghe, K.; Raman, E. P.; MacKerell, A. D. Automation of the CHARMM General Force Field (CGenFF) II: Assignment of Bonded Parameters and Partial Atomic Charges. *J. Chem. Inf. Model.* **2012**, *52* (12), 3155−3168.

(63) Vanommeslaeghe, K.; MacKerell, A. D. Automation of the CHARMM General Force Field (CGenFF) I: Bond Perception and Atom Typing. *J. Chem. Inf. Model.* **2012**, *52* (12), 3144−3154.

(64) Huang, J.; Rauscher, S.; Nawrocki, G.; Ran, T.; Feig, M.; de Groot, B. L.; Grubmüller, H.; MacKerell, A. D. CHARMM36m: An Improved Force Field for Folded and Intrinsically Disordered Proteins. *Nat. Methods* **2017**, *14* (1), 71−73.

(65) Klauda, J. B.; Venable, R. M.; Vorobyov, I.; MacKerrell, A. D.; Pastor, R. W. Update of the CHARMM All-Atom Additive Force Field for Lipids: Validation on Six Lipid Types. *J. Phys. Chem. B* **2010**, *114* (23), 7830.

(66) Berendsen, H. J. C.; Postma, J. P. M.; van Gunsteren, W. F.; DiNola, A.; Haak, J. R. Molecular Dynamics with Coupling to an External Bath. *J. Chem. Phys.* **1984**, *81* (8), 3684−3690.

(67) Darden, T. Particle mesh Ewald: An N·log(N) method for Ewald sums in large systems. *J. Chem. Phys.* **2021**, *98*, 10089.

(68) Hess, B.; Bekker, H.; Berendsen, H. J. C.; Fraaije, J. G. E. M. LINCS: A Linear Constraint Solver for Molecular Simulations. *J. Comput. Chem.* **1997**, *18* (12), 1463−1472.

(69) Humphrey, W.; Dalke, A.; Schulten, K. VMD: Visual Molecular Dynamics. *J. Mol. Graph.* **1996**, *14* (1), 33−38.

(70) Michaud-Agrawal, N.; Denning, E. J.; Woolf, T. B.; Beckstein, O. MDAnalysis: A Toolkit for the Analysis of Molecular Dynamics Simulations. *J. Comput. Chem.* **2011**, *32* (10), 2319−2327.

(71) McGibbon, R. T.; Beauchamp, K. A.; Harrigan, M. P.; Klein, C.; Swails, J. M.; Hernández, C. X.; Schwantes, C. R.; Wang, L.-P.; Lane, T. J.; Pande, V. S. MDTraj: A Modern Open Library for the Analysis of Molecular Dynamics Trajectories. *Biophys. J.* **2015**, *109* (8), 1528−1532.

(72) Research (CCR), C. for C. *Center for Computational Research Facility Description*; 2019.